Chapter 2

Theoretical Background

Since 1930s, many theories and discoveries in particle physics have revealed the fundamental structure of matter. The matter is made up of fundamental particles and their interactions are mediated by four fundamental forces [2]. The theoretical models strive to describe all the phenomena of particle physics and properties of particles. These models must be either confirmed experimentally or totally excluded giving hints of new physics. This interplay between experimental discoveries and the corresponding theoretical predictions leads to a theoretical model called Standard Model, which describes the fundamental particles and their interactions. The world's most powerful particle accelerators and detectors are used by physicists to test the predictions and limits of the Standard Model where it has successfully explained almost all experimental results. This chapter describes the Standard Model with main focus on the theory of strong interactions called Quantum Chromodynamics and its features which serve as the theoretical base of this thesis.

2.1 Standard Model

The Standard Model (SM) of particle physics [3–5] was developed in 1970s. It is a mathematical framework which describes the nature and properties of the fun-

damental particles and the three of the four known interactions between them, as summarized in Fig. 2.1. According to the SM, the basic constituents of matter are fermions and bosons. The fermions have half integral spin and obey Fermi-Dirac statistics. They follow the Pauli exclusion principle according to which two or more identical fermions cannot occupy the same quantum state. Each fermion has an associated anti-particle having the same properties but opposite-sign quantum numbers.

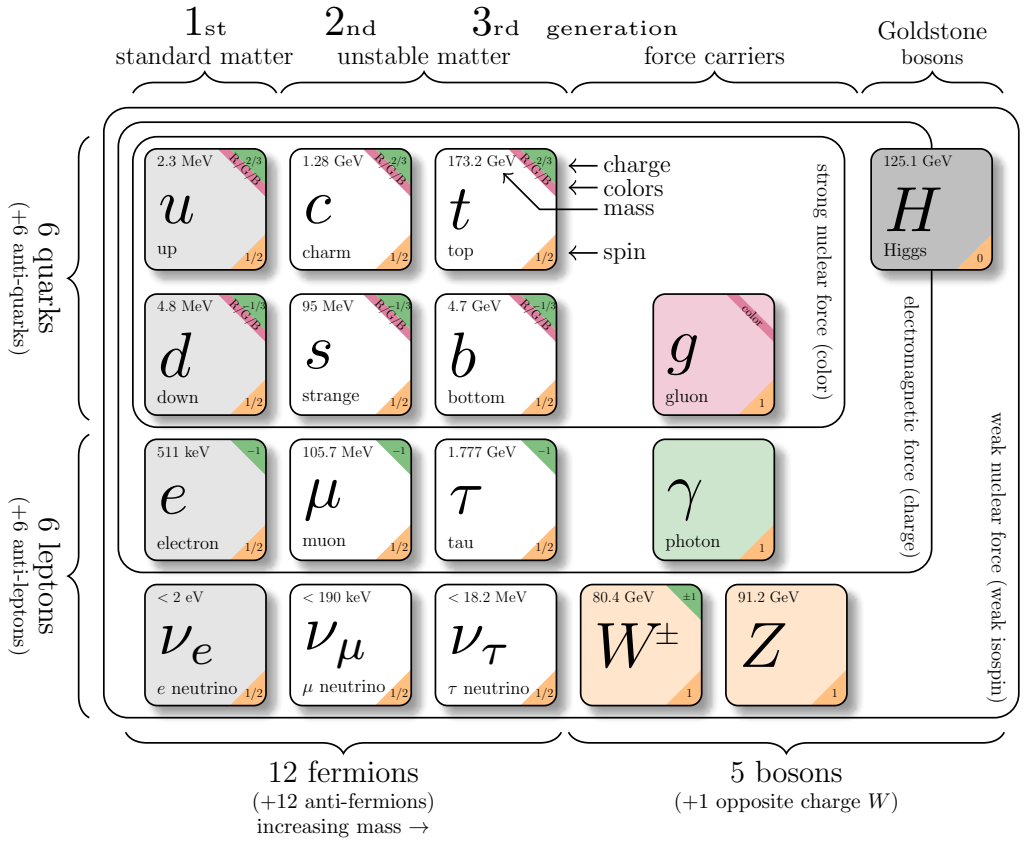

Figure 2.1: The Standard Model[3] summarizing the properties of elementary particles known as fermions (leptons and quarks) grouped into three generations, gauge bosons as mediators for the interactions and the scalar Higgs boson.

Depending on how the fermions interact, these are classified into two categories - leptons (ℓ) and quarks (q). The leptons are of six types : electron (e), muon (μ)

[3]Source : `http://www.texample.net/tikz/examples/model-physics`

and tau (τ) with electric charge Q = -1 and the corresponding neutrinos : electron neutrino (ν_e), muon neutrino (ν_μ) and tau neutrino (ν_τ) having electric charge Q = 0. The quarks exist in six "flavors" : up (u), down (d), strange (s), charm (c), bottom (b) and top (t). u, c and t carry electric charge Q = $+\frac{2}{3}$ whereas d, s and b carry Q = $-\frac{1}{3}$. The quarks and leptons are categorized into three generations. The first generation has the lightest and the most stable particles whereas the heavier and less stable particles belong to the second and third generations.

The elementary bosons have integral spin and obey the Bose-Einstein statistics. These are further of two types : gauge bosons having non-zero integral spin and a scalar boson with zero spin. The gauge bosons are the force carriers which mediate the electromagnetic, strong, weak and gravitational forces. Every interaction involves the exchange of a gauge boson : the massless photon (γ) for the electromagnetic force, massless gluons (g) for the strong force, massive $W^{\pm}$ and Z for the weak force and the graviton (not yet found) for the gravitational force. However, the gravitational force has not been incorporated into SM yet. Along with this, the existence of dark matter or dark energy and the matter-antimatter asymmetry are still missing pieces in the SM. The interaction between fundamental particles acts because of some peculiar property of the particles - charge for the electromagnetic force, color for the strong force and flavor for the weak force.

The SM framework based on quantum field theories [6] is described by $SU(3)_C \otimes SU(2)_L \otimes U(1)_Y$ gauge symmetry where C stands for the color charge, L for weak isospin and Y for hypercharge[4]. Here $SU(3)_C$, $SU(2)_L$ and $U(1)_Y$ terms give rise to strong, weak and electromagnetic forces, respectively. U(n) are the unitary and SU(n) are the special unitary groups of degree n. The $SU(3)_C$ term defines the strong interaction between quarks and gluons mediated by gluons, with the three degrees of freedom of the color charge (C). The electromagnetic interaction of

[4]Hypercharge Y = Q - T_3, where Q is the electric charge and and T_3 is the third component of weak isospin.

particles is explained by the most precise theory, today known as Quantum Electrodynamics (QED). In SM, the weak and electromagnetic interactions are combined by an electroweak symmetry theory [7,8], described by $SU(2)_L \otimes U(1)_Y$ gauge group. But this electroweak unification could not explain the occurrence of massive weak gauge bosons. This problem was solved by Higgs mechanism [9, 10]. The Higgs boson, named after Peter Higgs, is the field quantum of the Higgs field responsible for electroweak symmetry breaking. In SM, the Higgs field is a SU(2) doublet which is a scalar under Lorentz transformations. The coupling of the bosons to the scalar Higgs field causes the spontaneous symmetry breaking which triggers the Higgs mechanism. After symmetry breaking, three of the four degrees of freedom in the Higgs field interact with the three weak gauge bosons ($W^{\pm}$ and Z) and allows them to be massive, while the remaining one degree of freedom becomes the Higgs boson. Its existence was confirmed by the CMS [11] and ATLAS [12] collaborations in 2012, with properties consistent with the SM. In contrast to the electroweak symmetry, the $SU(3)_C$ of the strong interaction is an exact symmetry and hence the gluons are massless. The strong interaction between quarks and gluons is described by quantum chromodynamics (QCD), explained in detail in the next section.

2.2 Quantum Chromodynamics

The strong interactions between the quarks and gluons are described by a non-abelian gauge theory called quantum chromodynamics (QCD) [13, 14]. The gauge group of QCD is the special unitary group $SU(3)_C$ with color charges C as the generators of the gauge group. Color charge is the peculiar property of QCD and has a similar role as the electric charge in electromagnetic interactions. However, the mediator of electromagnetic interactions, i.e. the photon itself does not carry any electric charge whereas the gluon itself carry color charge. This allows the self coupling of gluons and hence makes the theory non-abelian. Both the quarks and

gluons carry three types of color charges : red (r), green (g) and blue (b), and three types of anti-color charges : anti-red ($\bar{r}$), anti-green ($\bar{g}$) and anti-blue ($\bar{b}$). The quarks carry a single color charge whereas gluons carry a combination of color charges. There are nine eigen states of gluons but one of them $\frac{1}{\sqrt{3}}(r\bar{r} + g\bar{g} + b\bar{b})$ is a totally symmetric color singlet which has no net color charge and does not take part in interaction. The remaining eight eigen states of the gluons are :

$$r\bar{b},\ r\bar{g},\ g\bar{r},\ g\bar{b},\ b\bar{g},\ b\bar{r},\ \frac{1}{\sqrt{2}}(r\bar{r}\ -\ b\bar{b}),\ \frac{1}{\sqrt{6}}(r\bar{r} + b\bar{b}\ -\ 2g\bar{g}) \tag{2.1}$$

The dynamics of the quarks and gluons are controlled by the gauge invariant QCD Lagrangian $\mathcal{L}_{QCD}$ which is composed of four terms as :

$$\mathcal{L}_{QCD} = \underbrace{-\frac{1}{4}F^{A}_{\mu\nu}F^{\mu\nu}_{A}}_{\mathcal{L}_{gluons}} + \underbrace{\sum_{flavors} \bar{q}_a\big(i\gamma^{\mu}(D_{\mu})_{ab}\ -\ m_q\big)q_b}_{\mathcal{L}_{quarks}} + \mathcal{L}_{gauge} + \mathcal{L}_{ghost} \tag{2.2}$$

where $\mathcal{L}_{gluons}$ describes the kinetic term of the gluon fields $\mathcal{A}^{A}_{\mu}$; $\mathcal{L}_{quarks}$ defines the interaction between spin-$\frac{1}{2}$ quark fields q_a of mass m_q and spin-1 gluon fields $\mathcal{A}^{A}_{\mu}$ summing over all presently known six flavors of quarks; $\mathcal{L}_{gauge}$ describes the chosen gauge and $\mathcal{L}_{ghost}$ is the so-called ghost term required to treat the degeneracy of equivalent gauge field configurations in non-abelian gauge theories. In Eq. 2.2, the Greek letters μ, ν, ... $\in$ {0,1,2,3} are the space-time indices; a,b,c $\in$ {1,2,3} and A,B,C $\in$ {1,...,8} are the indices of the color triplet and octet representations, respectively, of the gauge symmetry group $SU(3)_C$. The field tensor $F^{A}_{\mu\nu}$ is defined as

$$F^{A}_{\mu\nu} = \partial_{\mu}\mathcal{A}^{A}_{\nu} - \partial_{\nu}\mathcal{A}^{A}_{\mu} - g_s f^{ABC}\mathcal{A}^{B}_{\mu}\mathcal{A}^{C}_{\nu} \tag{2.3}$$

where g_s is the coupling constant determining the strength of the interaction between

colored partons and f^{ABC} are the structure constants of the $\mathrm{SU(3)_C}$ group. The last term in Eq. 2.3 is a non-abelian term which distinguishes QCD from QED and gives rise to a three- and a four-gluon vertex. In the term $\mathcal{L}_{quarks}$, $(D_\mu)_{ab}$ is the covariant derivative given by Eq. 2.4 and γ_μ are the Dirac γ-matrices.

$$(D_\mu)_{ab} = \partial_\mu \delta_{ab} + i g_s T^A_{ab} \mathcal{A}^A_\mu \tag{2.4}$$

$\mathcal{A}^A_\mu$ are the gluon fields with factors T^A_{ab} factors corresponding to the generators of the $\mathrm{SU(3)_C}$ gauge group. The generators are represented via $T^A = \lambda^A/2$ by the Hermitian and traceless Gell-Mann matrices λ^A [15]. The generator matrices T^A follow the commutation relations :

$$\left[T^A, T^B\right] = i f^{ABC} T^C \tag{2.5}$$

In $\mathcal{L}_{QCD}$, the classical contribution comes from $\mathcal{L}_{gluons}$ and $\mathcal{L}_{quarks}$ terms which give rise to the free quark- and gluon-field terms, and the quark-gluon interaction terms presented in Fig. 2.2. The cubic and quartic gluon self-interaction vertices proportional to g_s and g_s^2, respectively, come into play due to the non-abelian property of QCD.

It is impossible to use perturbation theory on a gauge invariant Lagrangian without choosing a specific gauge in which to calculate. The usual gauge-fixing term is given by

$$\mathcal{L}_{gauge} = -\frac{1}{2\xi}(\partial^\mu \mathcal{A}^A_\mu)^2 \tag{2.6}$$

where ξ may be any finite constant. This choice fixes the class of covariant gauges with ξ as the gauge parameter. As QCD is non-abelian, the gauge fixing term must

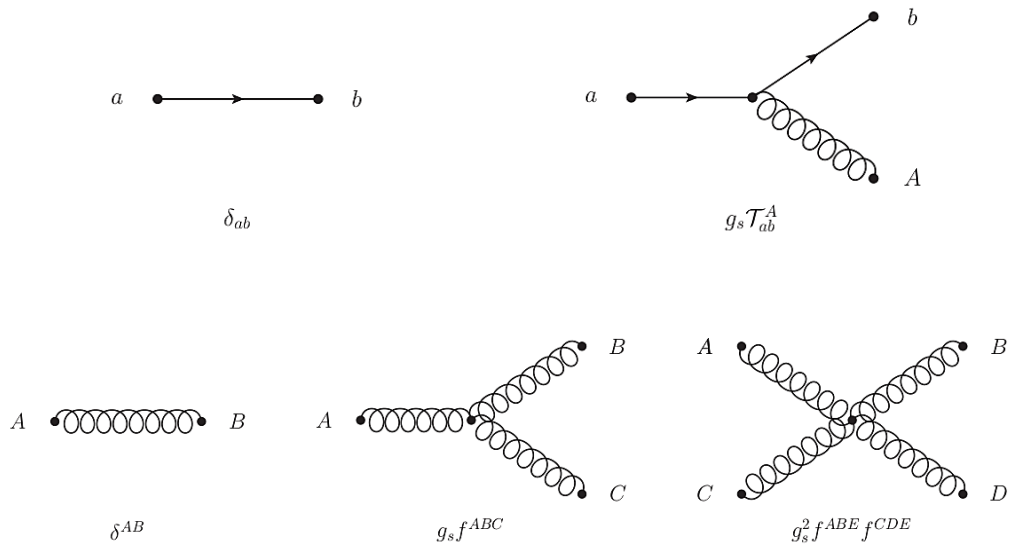

Figure 2.2: The fundamental Feynman rules of a free quark-field term (top left), quark-gluon interaction term (top right), free gluon-field term (bottom left), cubic gluon self-interaction term (bottom middle) and quartic gluon self-interaction term (bottom right). Taken from [16].

be supplemented by a ghost Lagrangian as

$$\mathcal{L}_{ghost} = \partial_\alpha \eta^{A\dagger}(D^\mu_{AB}\eta^B) \tag{2.7}$$

where η^A is a complex scalar field which obeys Fermi-Dirac statistics. The ghost fields cancel unphysical degrees of freedom arising due to use of covariant gauges. This completes the QCD Lagrangian shown in Eq. 2.2.

The strength of an interaction is given by a fundamental parameter called the coupling constant α. The electromagnetic coupling constant $\alpha_e = e^2/4\pi$, the weak coupling constant $\alpha_w = g_w^2/4\pi$ and the strong coupling constant $\alpha_S(Q) = g_s^2/4\pi$ are not constant and each depends on the separation between the interacting particles. In contrast to α_e, $\alpha_S(Q)$ increases with the increase in the distance or decrease in the energy scale Q, as shown in Fig. 2.3. α_w also increases with the increase in the distance but at a slower rate. At large distances or low energies, the quarks can never be found as free particles but exist in color neutral bound states known

as hadrons. Hadrons are of two types : baryons and mesons. According to the quark model [2] every (anti-)baryon is made up of three (anti-)quarks and every meson is made up of a quark-antiquark pair. When the colored partons within a hadron are pulled farther and farther apart, there is an increase in the strength of force between them. This results in creation of new quark-antiquark pairs making it impossible to liberate a free quark or gluon. This property of QCD is known as confinement according to which at low energy, the partons are forever bound into hadrons such as protons (uud), neutrons (udd) etc. Although the gluons are massless, the confinement leads to the finite range of the strong interactions. On the other hand, at small distances, the strength of coupling decreases. The quarks and gluons interact very weakly and behave as free particles. This property is known as asymptotic freedom. This indicates that perturbative theory is only applicable at high energies or small distances.

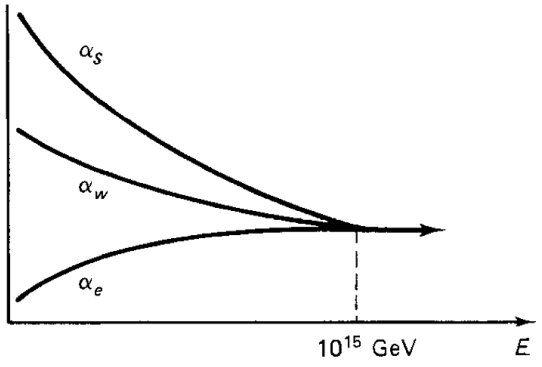

Figure 2.3: Evolution of three fundamental coupling constants : the strong coupling constant α_S, the weak coupling constant α_w and the electromagnetic coupling constant α_e. Taken from [2].

2.2.1 Perturbative Quantum Chromodynamics

At high energies, the property of asymptotic freedom allows a perturbative treatment in QCD calculations. In perturbative quantum chromodynamics (pQCD), a physical observable X such as cross-section of a scattering process, can be expanded as a

perturbative series in terms of coupling constant α_S as :

$$X = \sum_{i=0}^{N} \alpha_s^n \mathrm{c}_i = \mathrm{c}_0 + \alpha_s^1 \mathrm{c}_1 + \alpha_s^2 \mathrm{c}_2 + ... \tag{2.8}$$

where c_i are the perturbative coefficients. In a process, the pQCD calculation of X is determined by summing over the amplitudes of all Feynman diagrams contributing to that process. For a given Feynman diagram, the power of α_S is determined by the number of vertices associated with quark-gluon or gluon-gluon interactions. A leading order (LO) prediction sums over only the lowest-order contribution whereas next-to-leading order (NLO) includes terms with one additional power of α_S. The next-to-next-to-leading order (NNLO) includes emission of another gluon or a virtual gluon loop. The different orders in a $2 \rightarrow 2$ scattering process are shown in Fig. 2.4. The calculations become complex with the loop diagrams where the momenta of the virtual particles in a loop are not fully constrained by four-momentum conservation and the associated integrals are divergent. Such ultraviolet (UV) divergences enter the calculations beyond LO either due to loop or vertex corrections. These are overcome by a procedure known as renormalization, described in next section. Apart from the UV divergences, the QCD also suffers from infrared and collinear divergences (IRC) due to the presence of massless gluons and neglected quark masses. These need to be handled in pQCD calculations. The observable to be studied must be IRC safe.

2.2.2 Renormalization and Running of the Strong Coupling

The renormalization is a mathematical procedure which allows the finite calculation of momenta integrals of virtual loop by removing UV divergences. It introduces a regulator for the infinities, the renormalization scale μ_r. At first, the divergences are regularized temporarily by introducing a cut-off to the loop momenta at μ_r

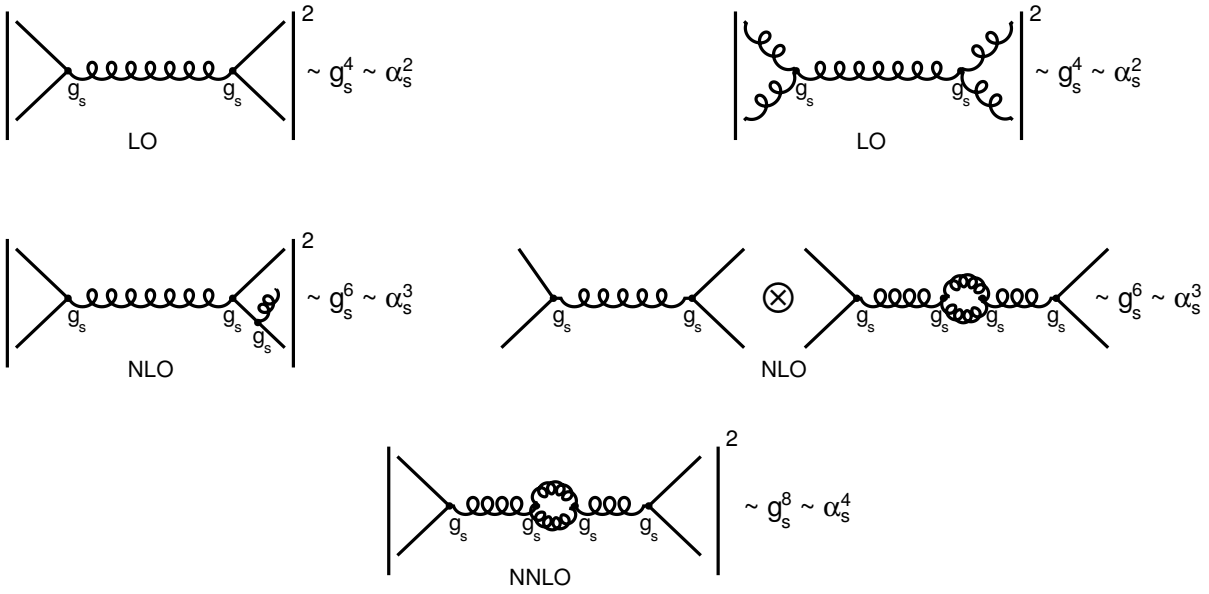

Figure 2.4: Feynman diagrams[5]of leading-order (LO), next-to-leading order (NLO) and next-to-next-to-leading order (NNLO) contributions of $2 \to 2$ scattering process.

scale. Then the free parameters of the Lagrangian, i.e. the coupling constant are redefined or renormalized to absorb the UV divergences. Due to this, both $\alpha_S(Q)$ and observable X become a function of μ_r. The exact dependence of $\alpha_S(\mu_r^2)$ on μ_r is described by the renormalization group equation (RGE) [17] which determines the running of $\alpha_S(\mu_r^2)$. According to RGE, the dependence of X on μ_r must cancel. Mathematically this can be expressed as :

$$\mu_r^2 \frac{d}{d\mu_r^2} X\left(\frac{Q^2}{\mu_r^2}, \alpha_s(\mu_r^2)\right) = \left(\mu_r^2 \frac{\partial}{\partial \mu_r^2} + \mu_r^2 \frac{\partial \alpha_s(\mu_r^2)}{\partial \mu_r^2} \frac{\partial}{\partial \alpha_s(\mu_r^2)}\right) X = 0 \qquad (2.9)$$

Using beta function $\beta(\alpha_S) = \mu_r^2 \frac{\partial \alpha_s(\mu_r^2)}{\partial \mu_r^2}$, Eq. 2.9 can be re-written as

$$\left(\mu_r^2 \frac{\partial}{\partial \mu_r^2} + \beta(\alpha_S) \frac{\partial}{\partial \alpha_s(\mu_r^2)}\right) X = 0 \qquad (2.10)$$

[5]Drawn using ROOT

By setting the renormalization scale equal to the physical scale i.e. $\mu^2 = Q^2$, $X\big(1, \alpha_s(Q)\big)$ is a solution to above equation where Q-dependence of X is only from the renormalization of the theory. Hence measuring the Q-dependence of X will directly probe the quantum structure of the theory. The β function in QCD has a perturbative expansion as :

$$\beta(\alpha_S) = -\alpha_s^2\Big(b_0 + b_1\alpha_S + b_2\alpha_s^2 + \mathcal{O}(\alpha_s^3)\Big) \tag{2.11}$$

where b_n is the $n+$ 1-loop β-function coefficients giving the dependence of the coupling on the energy scale Q. In the modified minimal subtraction ($\overline{\text{MS}}$) scheme [18, 19], the beta coefficient functions have following values :

$$b_0 = \frac{33 - 2n_f}{12\pi}, \quad b_1 = \frac{153 - 19n_f}{24\pi^2}, \quad b_2 = \frac{77139 - 15099n_f + 325n_f^2}{3456\pi^3} \tag{2.12}$$

where n_f is the number of quark flavors with masses $m_q < \mu_r$. On integration of Eq. 2.11, the energy dependence of α_S is yielded. Neglecting the higher orders, the first order solution of RGE is :

$$\alpha_s(\mu_r^2) = \frac{1}{b_0\,\ln(\mu_r^2/\Lambda_{QCD}^2)} \tag{2.13}$$

where Λ_{QCD} is the constant of integration. The perturbative coupling becomes large at the scale Λ_{QCD} and the perturbative series diverge. With $b_0 > 0$, the coupling becomes weaker at higher scales Q, i.e. the effective color charge is small at small distances or large energies. This allows the quarks to behave as free particles within the hadron, leading to the property called asymptotic freedom. It is always convenient to express α_S at some fixed scale. Since some of the best measurements come from Z decays, it is common practice to determine the strong coupling at the

scale of the Z boson mass $\alpha_s(M_Z)$. So, Eq. 2.13 can be expressed as :

$$\alpha_S\Big(\mu_r, \alpha_s(M_Z)\Big) = \frac{\alpha_s(M_Z)}{1+\ \alpha_s(M_Z) b_0 \ln(\mu_r^2/M_z^2)} \tag{2.14}$$

Since α_S is a free parameter of QCD theory, it must be extracted from experimental measurements and evolved to the scale of the Z boson. According to Particle Data Group (PDG) [20], the current world average value of the strong coupling constant at the scale of mass of Z boson is

$$\alpha_s(M_Z) = 0.1181 \pm 0.0011 \tag{2.15}$$

This value is derived using data from deep inelastic scattering process, electron-positron annihilation processes, hadronic τ lepton decays, lattice QCD calculations and electroweak precision fits. The different experimental determinations of the strong coupling constant evolved at the scale Q are shown as a function of Q in Fig. 2.5 which describe the running of the α_S up to the 1 TeV scale.

2.3 Hadronic Collisions

At large momentum transfer, the collision between two hadrons can be visualized as an interaction between their constituents - quarks and gluons. In this thesis, we are studying the proton-proton collisions taking place at the Large Hadron Collider (LHC). A proton is a complex composite particle consisting of three valence quarks (uud), gluons for the exchange of the strong force and the sea quarks. The sea quarks consist of quark-antiquark pairs coming into and out of existence rapidly and continuously due to gluon color field splitting. In any collision, a fundamental quantity to evaluate is the cross-section (σ) of a certain process which gives the probability that the two hadrons interact and give rise to that final state. In a

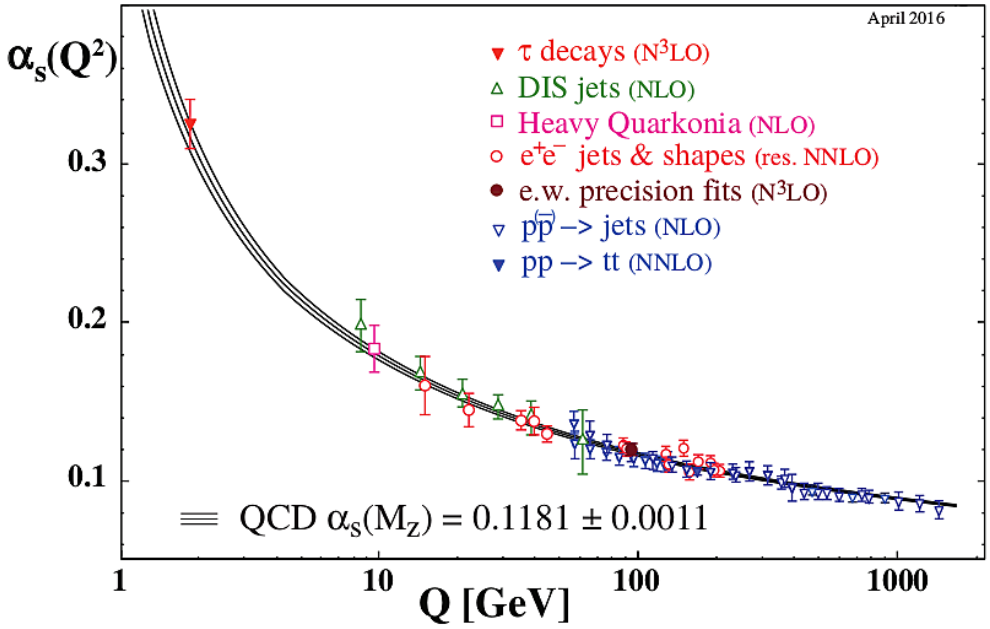

Figure 2.5: Different experimental determinations of the strong coupling constant α_S evolved at the energy scale Q are shown as a function of Q. These describe the running of the α_S up to the 1 TeV scale. Taken from [20].

hadronic collision, the perturbation theory is only valid at the parton-level but due to property of confinement at low energies, free partons cannot exist in nature. Only colorless hadrons can emerge as free particles from the high energy collisions. Here, the factorization theorem of QCD [21] comes into play which allows the calculation of σ by separating into two parts : a short-distance partonic cross-section calculable with pQCD, and a non-perturbative long-distance part described by parton distribution functions $f_i(x, \mu_f)$ (PDFs). The PDFs describe the partonic content of the colliding hadrons and give the probability to find a parton i with momentum fraction x within a hadron. μ_f is the factorization scale which corresponds to the resolution with which the hadron is being probed. The particles which are emitted with transverse momenta $p_{\mathrm{T}} > \mu_f$ are considered in the calculation of hard scattering perturbative coefficients. The particles emitted with $p_{\mathrm{T}} < \mu_f$ are accounted for within the PDFs. Applying the factorization theorem to a proton-proton collision,

the cross-section of a hard scattering process can be written as :

$$\sigma_{P_1P_2\to X} = \sum_{i,j} \int dx_1 dx_2 f_{i,P_1}(x_1,\mu_f) f_{j,P_2}(x_2,\mu_f) \times \hat{\sigma}_{ij\to X}\left(x_1p_1, x_2p_2, \alpha(\mu_r^2), \frac{Q^2}{\mu_f^2}\right) \tag{2.16}$$

where f_i and f_j are the proton PDFs which depend on momentum fractions x_1 and x_2 of parent protons P_1 and P_2 respectively as well as on the factorization scale μ_f. The sum extends over all contributing initial-state parton flavors $i,\ j$. The cross-section for the production of final state X at parton level ($\hat{\sigma}_{ij}$) depends on the final state phase space, the factorization scale μ_f and the renormalization scale μ_r. Figure 2.6 illustrates the factorization into the PDFs and the hard scattering cross-section in a proton-proton collision.

The PDFs of the proton are a necessary input to almost all theory predictions of a proton-proton collision. Perturbative QCD does not predict the parton content of the proton. So the shapes of PDFs are determined in fits to experimental measurements of different experiments. The dependence of PDFs on μ_f is given by the Dokshitzer-Gribov-Lipatov-Altarelli-Parisi (DGLAP) [22–24] equations which use α_S and the RGE as inputs. The knowledge of proton PDFs mainly comes from Deep-Inelastic-Scattering (DIS) HERA, fixed target and Tevatron data. The LHC data have a potential to improve constraints of the PDFs further as done in one of the recent CMS measurements [25]. There are several groups which determine the PDFs which mainly differ in choice of input data sets, treatment of heavy quarks, order of perturbation theory, way of treating experimental errors and theoretical assumptions. Global PDFs are the CTEQ [26], MMHT [27], NNPDF [28] and ABM [29] at LO, NLO and NNLO.

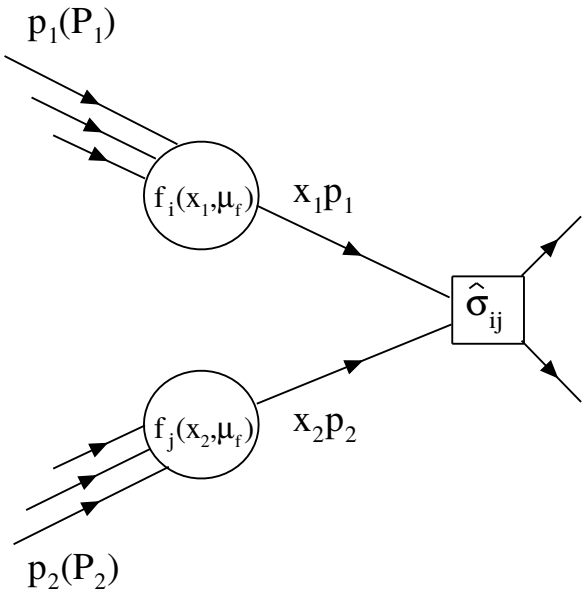

Figure 2.6: Schematic illustration[6]of the factorization theorem in a collision of two protons P1 and P2 having momenta p1 and p2, respectively. In a hard-scattering process at a scale Q^2, the two partons x_1 and x_2 participate with momenta x_1p_1 and x_2p_2. The total cross-section is factorized into the hard scattering cross-section $\hat{\sigma}_{ij}$ calculable using pQCD and the PDFs $f_i(x_1, \mu_f)$ and $f_j(x_2, \mu_f)$ with factorization scale μ_f.

2.3.1 Parton Shower and Hadronization

The partons involved in a hard scattering process get accelerated due to large momentum transfers. These accelerated partons emit QCD radiation in the form of gluons with successively lower energy. Unlike the uncharged photons in QED, the gluons themselves carry color charge and hence emit further gluons. The emitted gluons in turn can split into $q\bar{q}$ pairs. This successive emission of partons is described as a parton shower. In a parton shower, the main contribution is by the collinear parton splitting and the soft gluon emissions. The parton showers mimic the effect of higher-order corrections to the hard process. These cannot be calculated exactly and are taken into account using the parton shower approximation.

[6]Drawn using ROOT

The two incoming partons, which are constituents of two colliding hadrons and take part in hard scattering process, can also develop parton showers, commonly known as Initial-State Radiation (ISR). The initial partons produce showers till they collide to initiate the hard scattering process. The final outgoing partons produced from a hard scattering process can also undergo parton showering giving rise to Final-State Radiation (FSR). A parton shower terminates when the scale Q is below the hadronization scale $\sim$ 1 GeV for QCD.

At the end of the shower, there is a decrease in the energy of partons due to successive emission of gluons. Due to this, the coupling constant of QCD α_S grows large and pQCD is not applicable anymore. This leads to the confinement of colored quarks and gluons into the color-neutral composite particles called hadrons and this process is known as hadronization. The hadronization takes place at low momentum transfer and hence is non-perturbative in nature. Because no exact theory for hadronization is known, different phenomenological models have been developed to simulate the hadronization process. The two main models implemented in Monte Carlo (MC) event generators are :

Lund String Fragmentation Model - In the Lund string model of hadronization [30], the highly energetic gluons are treated as field lines. Due to the gluon self-interaction, the gluons are attracted to each other forming a narrow tube or string of strong color field between a $q\bar{q}$ pair. This model is based on an observation that at distances greater than about a femtometre (fm)[7], the potential energy $V(r)$ of colored quarks grows linearly with the increase in distance between them (r) as :

$$V(r) = \kappa r \tag{2.17}$$

where $\kappa \sim 1$ GeV/fm is the tension of the string connecting the quarks. When the q and $\bar{q}$ are pulled apart from each other, the gluonic string stretches. As a

[7] 1 femtometre = 1×10^{-15} metres

consequence, the potential energy of the string grows at the expense of the kinetic energy of the quarks. As the potential energy approaches the order of hadron masses, the string breaks at some point along its length, creating a new $q\bar{q}$ pair. The newly formed two string segments again stretch and break producing further $q\bar{q}$ pairs. This process of stretching and breaking continues until all the potential energy gets converted to $q\bar{q}$ pairs. This whole process is illustrated in Fig. 2.7. Subsequently, the $q\bar{q}$ pairs are transformed into final-state hadrons. The PYTHIA MC generator uses the Lund string fragmentation model.

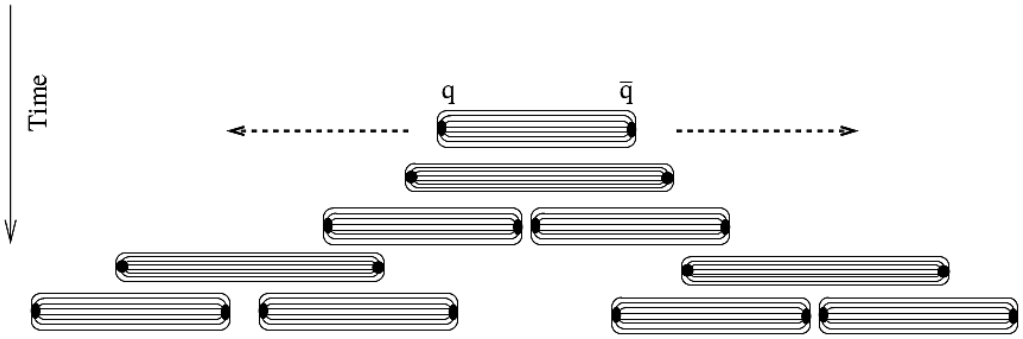

Figure 2.7: Illustration of the hadronization process in Lund string model[8]. When the quark q and anti-quark $\bar{q}$ are pulled apart from each other, the potential energy of the gluonic string connecting the quarks increases. As it becomes of the order of hadron masses, the string breaks and a new $q\bar{q}$ pair is created. The breaking of string and creation of $q\bar{q}$ continues till all the potential energy gets converted to $q\bar{q}$ pairs which then get hadronized.

Cluster Fragmentation Model - The cluster model of hadronization [31, 32] is based on preconfinement property of QCD [33]. According to this property, at evolution scales Q_0 much less than the hard process scale Q, the partons produced in a shower are clustered in colorless groups with an invariant mass distribution, depending on nature of hard process and Q_0, not on Q. This model contains two steps : firstly all gluons split into $q\bar{q}$ pairs at the end of the parton shower and in the second step, a new set of low-mass color-singlet clusters are obtained which decay into either secondary clusters or directly into hadrons. The generator HERWIG is

[8]Source : `http://inspirehep.net/record/806744`

based on the cluster fragmentation model.

2.3.2 Underlying Event

Due to the composite nature of the protons, the event structure is significantly more complex than that of the lepton collisions. The final states of the collisions involve multi-parton interactions. In a high energy proton-proton collisions, the underlying event (UE) includes the effects which are not coming from the primary hard scattering process. The UE includes the contributions from relatively small

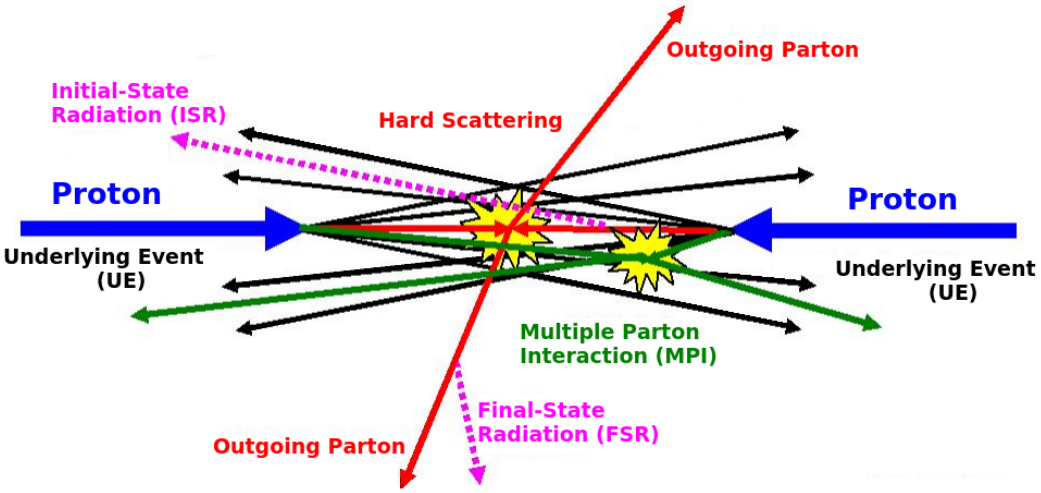

Figure 2.8: A proton-proton collision[9] involving the main hard scattering process along with the low momentum transfer underlying event (UE) contributions coming from initial- and final-state radiations (ISR and FSR) complemented with multiple parton interactions (MPI) and collisions from leftover partons called beam remnants.

momentum transfer processes : initial and final-state radiations (ISR, FSR), leftover partons in the collisions called beam remnants and multiple parton interactions (MPI). Due to composite nature of proton, the remaining two partons which do not participate in a hard collision may also interact giving rise to multiple parton interactions. The UE induces an additional energy in an event which is not related

[9]Source : `https://cds.cern.ch/record/1382404`

to the main interaction. This acts as an unavoidable background which needs to be removed. Hence, it is crucial to study and understand the UE. The UE activity increases with Q and the center-of-mass energy $\sqrt{s}$. Figure 2.8 shows the complex variety of processes taking place in a single proton-proton collision.

2.4 Jets

The bunch of hadrons, produced from hadronization of quarks and gluons, gets collimated in the form of "jets" with the direction towards the direction of the initial parton that originated them. The jets [34] are conical structures which group hadrons into a single physics entity and can be observed experimentally in the detectors. These act as a bridge between the elementary quarks and gluons of QCD and the final hadrons produced in high energy collisions. The jet structure was observed for the first time in hadron production of e^+e^- annihilation process at SLAC in 1975 [35]. Figure 2.9 shows the the outgoing partons of the hard scattering process in a proton-proton collision, undergoing fragmentation and hadronization processes and forming a conical jet with radius R.

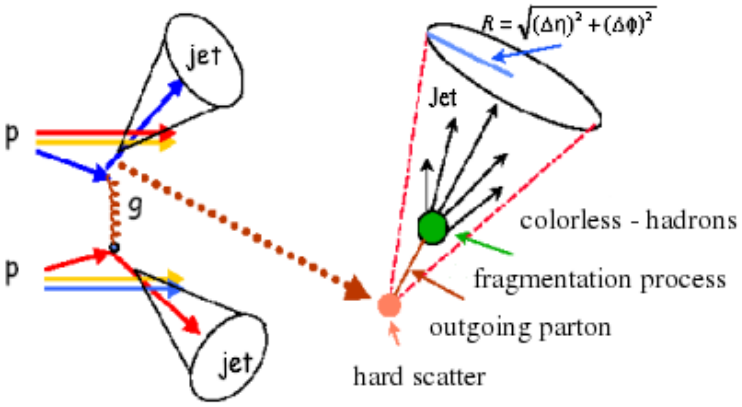

Figure 2.9: In a proton-proton collision, the outgoing partons of the hard scattering process undergo fragmentation and hadronization processes producing a shower of partons which get collimated into a conical jet with radius R.

The partons can not be measured directly by the experiments because they can not exist freely in nature. The information about the dynamics of the partons can be obtained indirectly from jets. The configurations of high-energy quarks and gluons at short distances are reflected in the energy and angular distributions of the jets. Hence, the jets are important to study. Therefore, at large momentum transfer of the interacting partons, the jets and their observables are the best tools to test the predictions of pQCD. Also, the jet production is sensitive to the strong coupling constant α_S. The precise knowledge of the jet production cross-section can help to extract the value of α_S and also to reduce the uncertainties of the PDFs of the proton. At the LHC, the simplest jet production process is a $2 \rightarrow 2$ scattering process giving dijet events, whereas $2 \rightarrow 3$, $2 \rightarrow 4$ parton reactions in pQCD give rise to multijet events. The investigation of inclusive multijet event cross-sections permits more elaborate tests of QCD. Also, a precise study of jet variables helps to understand the signal and background modelling for new physics searches in hadronic final states. In this thesis, the inclusive multijet event cross-sections as well as the ratio of cross-sections are exploited to extract the value of the strong coupling constant α_S. In the next section, we focus on the definition of a jet.

2.4.1 Jet Algorithms

Jet algorithms [36] provide a set of rules which determine how the particles can be clustered into a jet. In a jet algorithm, usually one or more parameters are involved that indicate how close two particles must be for them to belong to the same jet. These parameters can either measure closeness in coordinate space (cone algorithms) or in momentum space (sequential recombination algorithms). The jet algorithms are applicable on parton, particle and detector levels. A recombination scheme is always associated with a jet algorithm which calculates the momentum assigned to the combined particles. A jet algorithm along with its parameters and a recombination scheme forms a "jet definition". A jet definition [37] must be simple to implement

in an experimental analysis as well as in the theoretical calculation. It should be defined at any order of perturbation theory and must yield finite cross-sections that are relatively insensitive to hadronization. In addition to these requirements, a jet algorithm must be infrared and collinear (IRC) safe. Infrared safety is the property by which the addition of a soft emission i.e. addition of a soft gluon should not change or modify the number of hard jets found in an event. In an infrared unsafe algorithm, a soft gluon emission in the middle of two cone jets can lead to overlap of the two initial cones, as shown in Fig. 2.10 (top). This produces a single jet instead

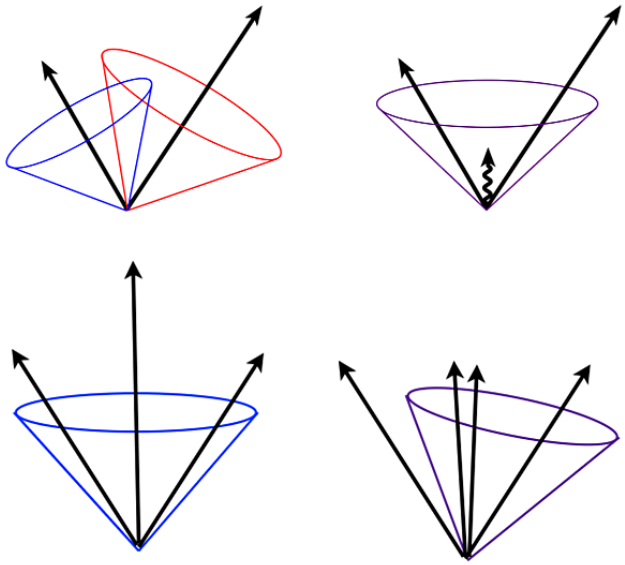

Figure 2.10: Top : Infrared unsafe behaviour of jet algorithm is illustrated where the presence of soft radiation between two jets may cause a merging of the jets that would not occur in the absence of the soft radiation. Bottom : Collinear unsafe behavior of jet algorithm is shown in which the number of jets change due to a collinear splitting[10].

of initial two jets resulting in the change of number of jets. Collinear safety is the property by virtue of which the collinear splitting i.e. replacement of one parton by two at the same place should not modify the number of jets formed in an event. This implies that the output of the jet algorithm should remain the same if the energy of a particle is distributed among two collinear particles. According to the collinear

[10]Source : `http://inspirehep.net/record/1251416`

safety property, the two cases shown in Fig. 2.10 (bottom) should always produce a single jet. If an algorithm produces zero or two jets after collinear splitting, then it is not collinear safe. The jet algorithms can be classified mainly into two types :

Cone Algorithms - In the iterative cone (IC) algorithm [38], the jet is defined as a cone with fixed radius R in η-ϕ space drawn around the highest energy seed. The relative distance (d) of all the particles is iteratively calculated and compared with R. If the calculated $d < R$, the considered particles are clustered together in a jet and the directions of the clustered particles give the direction of the jet. On the other side i.e. if $d > R$, the considered particles initiate two different jets. The algorithm iterates until the cone is stable which means that the direction of sum of momentum of all the particles is same as that of the center of cone. But IC algorithm is not IRC safe. There is an another cone algorithm, Seedless Infrared-Safe cone (SIS-Cone) [39], which is an exact seedless i.e. does not rely on seed threshold and is IRC safe. This is a complex approach which tests the stability of all subsets of particles and has a complexity of $\mathcal{O}(N2^N)$ for N particles. But this algorithm is much slower and hence not preferred.

Sequential Recombination Algorithms - The sequential recombination algorithms [40] cluster the particles by defining a distance between pairs of particles and recombine the pair of closest particles successively. This is collinear and infrared safe algorithm. It is possible for cone jets to overlap such that one particle is contained in more than one jet but the sequential recombination algorithm never assigns a particle to more than one jet. The sequential recombination algorithm is based on transverse momentum p_{T} of the particles and follows the procedure as below :

1. First the distance d_{ij} between two particles i and j and distance d_{iB} of the particle to the beam are calculated.

$$d_{ij} = \min\left(p_{\mathrm{T}i}^{2p}, p_{\mathrm{T}j}^{2p}\right)\frac{\Delta R_{ij}^2}{R^2}, \qquad d_{iB} = p_{\mathrm{T}i}^{2p}$$
$$\text{where} \quad \Delta R_{ij}^2 = (y_i - y_j)^2 + (\phi_i - \phi_j)^2 \tag{2.18}$$

2. If $d_{ij} < d_{iB}$, then the particles i and j are merged into a new single jet object k, summing four-momenta of two initial particles by recombination scheme and step 1 is repeated.

3. If $d_{iB} < d_{ij}$, particle i is declared as a final-state jet and the particle gets removed from the list.

This procedure continues until all particles get clustered into jets. The value of the parameter p defines the three different sequential algorithms having distinct properties. For $p = 1$, we have k_t algorithm [41, 42], $p = 0$ gives the Cambridge/Aachen (C/A) algorithm [43] whereas p = -1 defines the anti-k_T algorithm [44]. The k_t algorithm involves clustering of soft particles first resulting in an area that fluctuates considerably. This algorithm is susceptible to the underlying and pileup events. The C/A algorithm involves energy independent clusterings. Both k_t and C/A produce jets of irregular shapes. Instead of jet analysis, these are widely considered for studying the jet substructure. The anti-k_T algorithm tends to cluster hard particles first and produces jets with more regular circular shapes. It is less sensitive to underlying and pileup events. It is the most preferred algorithm for jet studies at the LHC. Figure 2.11 shows the clustering of same particles but using the different jet algorithms.

A jet algorithm must specify how to combine the momenta of different partons or particles going to be clustered into a jet. This is given by the recombination scheme. The most widely used recombination scheme is the E-scheme [38] which corresponds to vector addition of four-momenta where the four-momenta of the jet is obtained by simply adding the four-momenta vectors of merging particles.

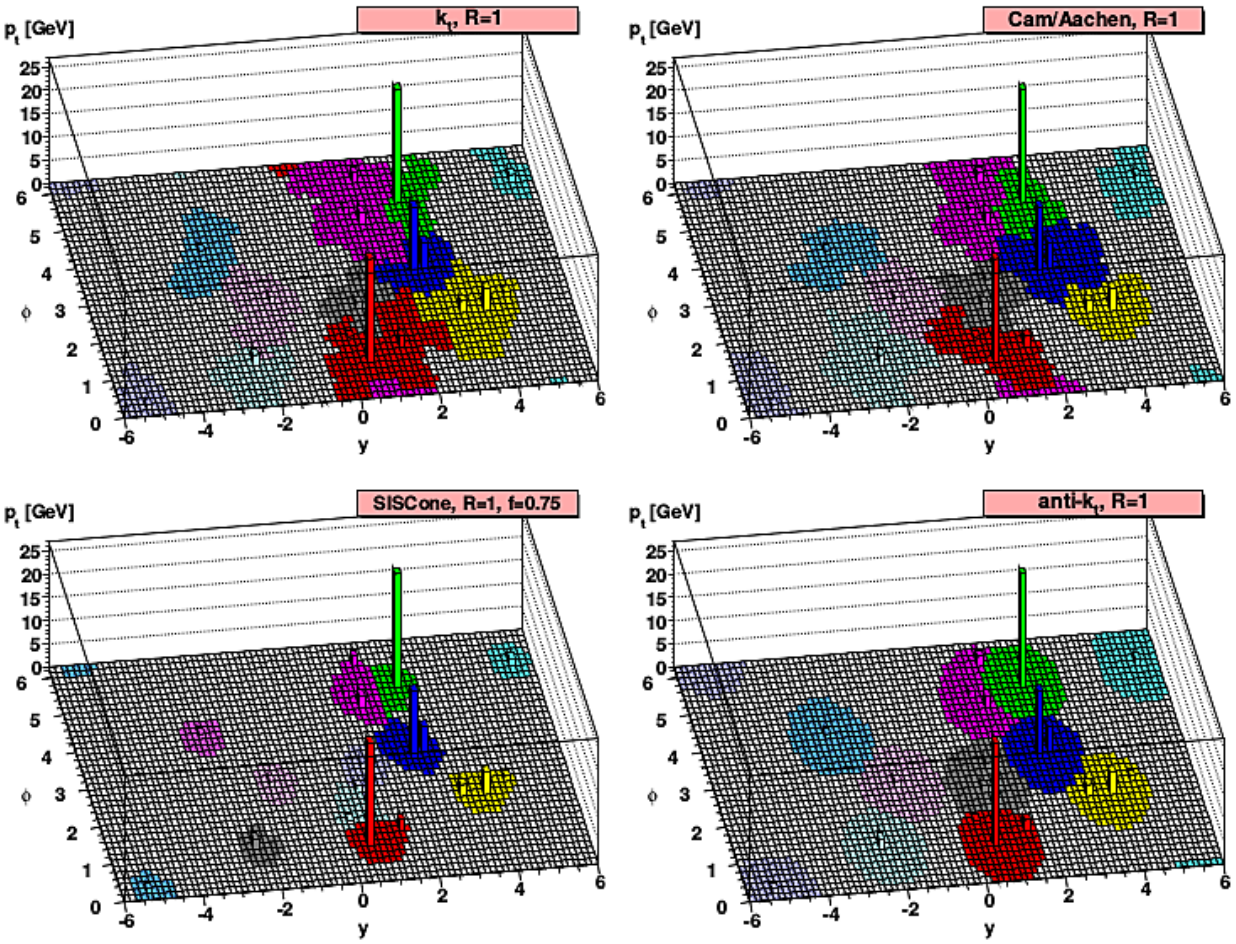

Figure 2.11: The clustering of particles, in y-ϕ space at the parton level, into jets clustered with the k_t (top left), Cambridge/Aachen (top right), SISCone (bottom left) and anti-k_t (bottom right) algorithms with $R = 1$. The towers represent the jet p_T. The anti-k_t algorithm gives circular jets while the jets produced with other three algorithms have irregular shapes. Taken from [36].

The sequential clustering algorithms have traditionally been favoured by theorists but not by experimentalists because of slow computational performance. However, the introduction of the FastJet program [45] enhanced the speed of clustering algorithms and hence are preferred by experimentalists as well. This thesis details the particles produced in proton-proton collisions by clustering them in to jets using anti-k_t algorithm with distance parameter $R = 0.7$. These jets are observed in the Compact Muon Solenoid detector of the Large Hadron Collider, the details of which are discussed in the following chapter.